Since January 2020 Elsevier has created a COVID-19 resource centre with free information in English and Mandarin on the novel coronavirus COVID-19. The COVID-19 resource centre is hosted on Elsevier Connect, the company's public news and information website.

Virology 380 (2008) 312–321

Contents lists available at ScienceDirect

Virology

journal homepage: www.elsevier.com/locate/yviro

An immunosuppressed Syrian golden hamster model for SARS-CoV infection

Scott R. Schaecher [a], Jennifer Stabenow [b], Christina Oberle [b], Jill Schriewer [b], R. Mark Buller [b], John E. Sagartz [c], Andrew Pekosz [d,*]

[a] Department of Molecular Microbiology, Washington University School of Medicine, 660 S. Euclid Avenue, St. Louis, MO 63110-1093, USA
[b] Department of Molecular Microbiology and Immunology, Saint Louis University Doisy Research Center, 1100 South Grand Boulevard, St. Louis, MO 63104, USA
[c] Seventh Wave Laboratories, Suite 209, 743 Spirit 40 Park Drive, Chesterfield, MO 63005, USA
[d] W. Harry Feinstone Department of Molecular Microbiology and Immunology, Johns Hopkins University, Bloomberg School of Public Health, 615 North Wolfe Street Suite E5132, Baltimore, MD 21205, USA

ARTICLE INFO

Article history:
Received 28 May 2008
Returned to author for revision 15 July 2008
Accepted 17 July 2008
Available online 28 August 2008

Keywords:
SARS-CoV
Coronavirus
Cyclophosphamide
ORF7a
ORF7b
Hamster
Accessory gene
Pathogenesis

ABSTRACT

Several small animal models have been developed for the study of severe acute respiratory syndrome coronavirus (SARS-CoV) replication and pathogenesis. Syrian golden hamsters are among the best small animal models, though little clinical illness and no mortality are observed after virus infection. Cyclophosphamide was used to immunosuppress hamsters leading to a prolonged disease course and higher mortality after SARS-CoV infection. In addition, there was a significant weight loss, expanded tissue tropism, and increased viral pathology in the lung, heart, kidney, and nasal turbinate tissues. Infection with recombinant SARS-CoV viruses bearing disruptions in the gene 7 coding region showed no significant change in replication kinetics, tissue tropism, morbidity, or mortality suggesting that the ORF7a (7a) and ORF7b (7b) proteins are not required for virus replication in immunosuppressed hamsters. This modified hamster model may provide a useful tool for SARS-CoV pathogenesis studies, evaluation of antiviral therapy, and analysis of additional SARS-CoV mutants.

Introduction

The severe acute respiratory syndrome coronavirus (SARS-CoV) emerged as the causative agent of a severe, atypical pneumonia in November, 2002. The disease first appeared in the Guangdong province of southeast China and rapidly spread to Hong Kong, Taiwan, Singapore, and over 30 other countries on six continents. By the end of the epidemic, over 8000 cases were reported with an overall mortality rate of approximately 10% (CDC, 2003). Although the precise origin of the virus has not been elucidated, evidence suggests that the virus likely was transmitted from bats in China through an intermediate host such as the masked palm civet to humans (Lau et al., 2005; Li et al., 2005; Ren et al., 2006).

The predominant mechanism for transmission is via airborne droplets, although isolation of virus from feces and urine may suggest additional routes of transmission (Chan et al., 2004a; Poon et al., 2004). Following inoculation, the virus undergoes an incubation period of 2–14 days (Chan et al., 2004b). Patients subsequently present with flu-like symptoms, fever, malaise, nonproductive cough, and progressive respiratory deterioration, typically with involvement of both lungs (Cheng et al., 2007; Gu and Korteweg, 2007). Patients often presented with watery diarrhea and hepatic dysfunction; 20–30% of patients developed respiratory failure and required mechanical ventilation.

Mortality in patients under 60 years of age was approximately 6.8%; however, disease severity was significantly increased in elderly populations with the mortality rate among individuals above 60 years of age approaching 50%, likely due to an ineffective antiviral immune response. Disease severity was shown to correlate with the early onset of neutralizing antibody responses; the presence of neutralizing antibody within the first two weeks of illness was associated with increased risk of mortality (Ho et al., 2005; Zhang et al., 2006). Recovering patients continued to increase serum neutralizing antibody concentrations, peaking at approximately day 20, whereas fatal cases demonstrated dramatically reduced neutralizing antibody after day 15 of symptom onset (Zhang et al., 2006). This suggests that sustainable levels of neutralizing antibody are correlated with recovery of SARS-CoV-infected patients.

Since the identification of the virus that causes SARS, numerous animal models have been described in attempts to evaluate virus replication, pathogenesis, and immunopathology. Animal models described to date include several inbred mouse strains, hamsters, civet cats, ferrets, cats, or nonhuman primates (Fouchier et al., 2003; Glass et al., 2004; Greenough et al., 2005; Hogan et al., 2004; Lawler et al., 2006; Martina et al., 2003; McAuliffe et al., 2004; Qin et al., 2005;

* Corresponding author. Fax: +1 410 955 0105.
E-mail address: apekosz@jhsph.edu (A. Pekosz).

0042-6822/$ – see front matter © 2008 Elsevier Inc. All rights reserved.
doi:10.1016/j.virol.2008.07.026

Roberts et al., 2005a; 2005b; 2007; Rowe et al., 2004a; Subbarao et al., 2004; ter Meulen et al., 2004; Wu et al., 2005). The timecourse of virus replication in these small animal models is significantly more rapid than that observed in human infections (Roberts et al., 2008) and no model fully reproduces the clinical illness or the pathology observed in humans. The need exists for a useful small animal model that more closely mimics human disease.

SARS-CoV infection of Syrian golden hamsters leads to viral replication in the lungs and nasal turbinates, transient viremia and extrapulmonary replication in the spleen and liver (Roberts et al., 2005b). Primary hamster tracheobronchial epithelial cell cultures support higher virus replication in comparison to similar murine cultures, suggesting an increased susceptibility of hamster cells to SARS-CoV infection (Sims et al., 2005). Histopathological evidence of disease is evident in hamster tissues, with cellular necrosis, pronounced interstitial inflammation, focal consolidation in pulmonary tissues, and loss of ciliated epithelial cells being prominent features (Roberts et al., 2005b); however, there is limited morbidity and no mortality associated with infection. Increasing the severity of disease in the hamster model may provide a useful tool for study of SARS-CoV pathogenesis, antiviral drug testing, and for analysis of mutant viruses deleted of one or more of the eight viral accessory genes.

Here, we report a cyclophosphamide (CP)-induced immunosuppressed Syrian golden hamster model for SARS-CoV infection. Cyclophosphamide, a bifunctional alkylating agent, has been shown to cause lymphopenia, suppress B-cell activity and activation, and suppress regulatory T-cell function (Cupps, et al., 1982; Ikezawa et al., 2005; Polak and Turk, 1974; Zhu et al., 1987). CP has been utilized in various animal models for virus infection analysis, often increasing the morbidity and mortality observed in virus-infected animals (Blandford and Charlton, 1977; Genovesi and Peters, 1987; Kercher and Mitchell, 2000; Kong et al., 2005; Mateo et al., 2006; Sidwell et al., 2003; Smee et al., 1991). Recently, CP-induced immunosuppression of Syrian golden hamsters was shown to enhance adenovirus replication and pathology, and permitted the efficacy testing of a broad-spectrum antiviral, CMX001 (Toth et al., 2008).

Treatment of hamsters with CP augmented virus-induced pathology and replication of recombinant SARS-CoV (rSARS-CoV) in tissues including lung, spleen, liver, kidney, and heart. Infected animals displayed high morbidity and mortality over approximately 30 days in a manner dependent on the dosage regimen of CP. A similar infection and pathogenesis pattern was observed after infection with rSARS-CoV mutants defective for the expression of accessory proteins ORF7a and ORF7b suggesting the functions of these proteins are not required in this model. Therefore, we propose infection of CP-treated hamsters as a more rigorous test of in vivo virus replication and virulence than that provided by existing animal models.

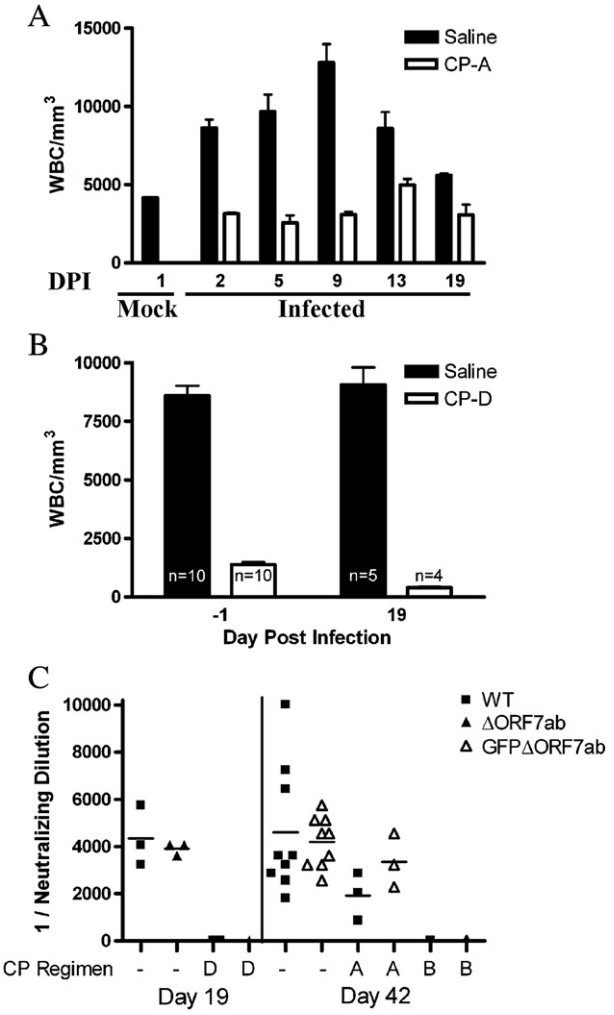

Fig. 1. Cyclophosphamide treatment results in immunosuppression of Syrian golden hamsters. (A) White blood cell (WBC) counts per mm^3 from saline or CP-A treated hamsters were determined in uninfected (mock) or rSARS-CoV infected animals. Data points are from $n=1$ mock infected, and $n=2$–6 for all other samples. The WBC counts in saline-treated, mock infected animals did not change significantly over the course of the experiment. The average and standard error are graphed. (B) Complete WBC counts per mm^3 at days-1 and 19 pi from saline or CP-D treated hamsters infected with rSARS-CoV. The average and standard error are graphed. (C) Serum neutralizing antibody titers from saline or CP-treated hamsters either mock infected or infected with the indicated recombinant SARS-CoV. Serum was collected from animals at days 19 and 42 pi, heat inactivated, and serial dilutions were assayed for neutralizing capacity against 100 $TCID_{50}$ of SARS-CoV. Data represent mean neutralizing titers.

Results

Cyclophosphamide induced immunosuppression in hamsters

To examine the effect of CP on the severity of rSARS-CoV disease in hamsters, groups of animals were assigned to either saline or one of four different CP regimens (Table 1). The four regimens were utilized to determine dose- and time-dependent effects of CP treatment on the severity of disease. Animals were given a loading dose followed by maintenance doses at specified intervals to maintain immunosuppression. To monitor the effect of treatments, total white blood cell counts measured in blood from mock infected animals or rSARS-CoV infected animals treated with saline, CP-A, or CP-D prior to infection and at various times through the study (Figs. 1A,B). Decreased white blood cells counts in animals treated with CP confirmed the immunosuppressive activity of the treatment regimens.

Table 1
Cyclophosphamide dosing regimens

Regimen	1st dose	Subsequent doses
Saline	0.8 mL saline at day-5	0.8 mL saline every 4 days
CP-A	70 mg/kg CP at day-2	50 mg/kg CP every 4 days
CP-B	140 mg/kg CP at day-5	100 mg/kg CP every 4 days
CP-C	140 mg/kg CP at day-2	100 mg/kg CP every 4 days
CP-D	140 mg/kg CP at day-5	100 mg/kg CP every 3 days

CP was administered intraperitoneally.

Animals were infected intranasally with 10^3 $TCID_{50}$ of rSARS-CoV, rSARS-CoV GFPΔORF7ab (a virus encoding GFP in place of the gene 7 open reading frame), or rSARS-CoV ΔORF7ab (a virus encoding a deletion of the gene 7 open reading frames) at day 0 (Schaecher et al., 2007b; Yount et al., 2005). Saline-treated animals demonstrated elevated total WBC counts and lymphocytosis that peaked on day 9 postinfection (pi), and returned to near baseline levels by day 19 pi (Fig. 1A). Treatment with the most mild CP regimen, CP-A, resulted in significant immunosuppression with animals demonstrating lower initial WBC counts after virus infection, when compared to saline-

treated animals (Fig. 1A). Animals treated with CP-D had depressed total WBC counts at day 1 compared to saline-treated animals with mean WBC counts of 1380±346 and 8590±1346 WBC/mm^3, respectively (Fig. 1B). By day 19 pi, mean WBC counts in CP-D treated animals dropped to 400±82 WBC/mm^3 compared to near baseline levels of 9060±1653 WBC/mm^3 in saline-treated animals.

SARS-CoV specific serum antibody response

To further confirm immunosuppression and analyze adaptive immune responses to rSARS-CoV, serum neutralizing antibodies specific for SARS-CoV were quantified on days 19 and 42 pi (Fig. 1C) using a virus neutralization assay. Saline-treated animals developed a high neutralizing antibody titer by day 19 pi with no significant difference observed between animals infected with different rSARS-CoV viruses. In contrast, little or no neutralizing antibody was detected in CP-D treated animals at day 19 pi. At day 42 pi, animals treated with CP-A had detectable neutralizing antibody responses to both viruses; however, mean neutralizing titers were 40% lower than those observed with saline-treated animals (1:4398±2008 and 1:2639±1244, respectively). No neutralizing antibody was detected in uninfected animals or virus-infected animals treated with CP-B

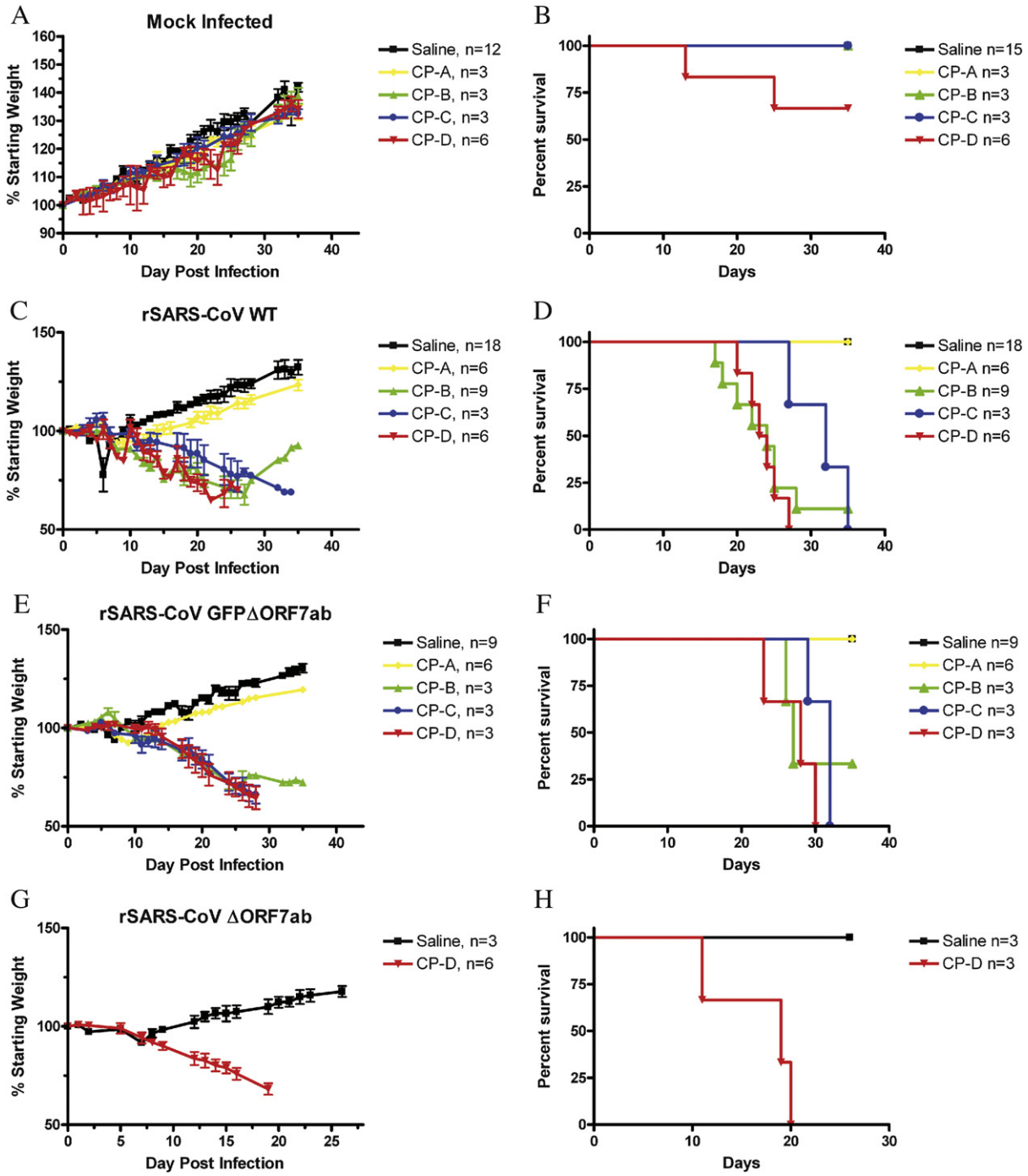

Fig. 2. Daily mean weight and survival of saline and cyclophosphamide treated hamsters infected with rSARS-CoV. Groups of 3 golden Syrian hamsters were dosed with CP per the regimen specified in Table 1 and inoculated intranasally with either saline (A,B) or 10^3 $TCID_{50}$ of rSARS-CoV (C,D), rSARS-CoV GFPΔORF7ab (E,F), or rSARS-CoV ΔORF7ab (G,H). Individual animals were weighed and data was normalized to animal weight on day 0 (A,C,E,G). Data represent average normalized weight and standard error. Percent survival of mock or CP-treated animals infected with each virus is shown (B,D,F,H). Black line, saline treatment; yellow line, CP-A; green line, CP-B; blue line, CP-C; red line, CP-D.

(animals treated with regimen CP-C were not analyzed for neutralizing antibody titer).

Clinical manifestations and mortality

Animals were monitored for morbidity and mortality (Fig. 2) over the course of approximately 36 days. Mock infected animals treated with any of the CP regimens demonstrated no significant weight loss or overt clinical illness compared to saline-treated, uninfected hamsters (Fig. 2A). With the exception of two out of six CP-D treated animals, no mortality was observed (Fig. 2B), indicating that CP treatment for less than 40 days had little impact on viability.

As observed previously (Roberts et al., 2005b; Schaecher et al., 2007b), SARS-CoV infection of hamsters resulted in minimal clinical illness and transient or no weight loss between days 5–7 pi (Figs. 2C,E, G). No mortality was observed in saline-treated hamsters (black line) infected with any virus. Virus infection of CP-A treated animals (yellow line) resulted in modest weight loss coupled with modest clinical symptoms (fur ruffling, decreased activity) compared to virus-infected, saline-treated hamsters, but resulted in no increase in mortality. In contrast, infection of CP-B (green line), CP-C (blue line), and CP-D (red line) treated animals resulted in an increased weight loss and mortality. Two of 12 CP-B treated and infected animals survived beyond day 28 and demonstrated some clinical improvement and weight gain. Infected animals treated with CP-C or CP-D progressively lost weight throughout approximately 30 days; no statistically significant difference in weight loss was observed among the treatment groups. Infection with viruses bearing disruptions of accessory gene 7 led to morbidity and mortality similar to that seen with wild-type virus, indicating that the disruption of gene 7 did not significantly alter virulence in this animal model.

Tissue tropism and virological analysis

Tissues were analyzed at various times pi for virus titers. Lungs from saline and CP-A treated animals contained high virus titers as early as day 2 pi, and titers remained high through day 5 (data not shown). By day 9 pi, saline-treated animals had cleared detectable virus from lung tissues while two of three CP-A treated animals continued to have high lung viral titers out to day 19 pi. No extrapulmonary virus was detected by $TCID_{50}$ analysis in saline-treated animals but virus titers were detected in several liver tissues harvested from CP-A treated, infected animals at days 5 and 9 pi (data not shown). Virus was not detected in any other tissues from CP-A treated animals.

Tissues from CP-B treated animals were analyzed at days 2, 5, and 9 pi (Fig. 3A). Lung titers in both saline and CP-B treated animals were high on days 2 and 5. No virus was detected in the lungs of saline-treated animals after day 5 pi; however, CP-B treated animals were unable to clear virus from the lung and titers remained high at day 9. Progressively increasing virus titers were detected in the liver and spleen of CP-B treated animals but not saline-treated animals.

High virus titers were present in lung, liver, spleen, and kidney tissues on day 19 pi in CP-D treated animals but no virus was detected in saline-treated animals (Fig. 3B). The presence of virus titers in kidney tissues is significant, as SARS-CoV has been detected in the

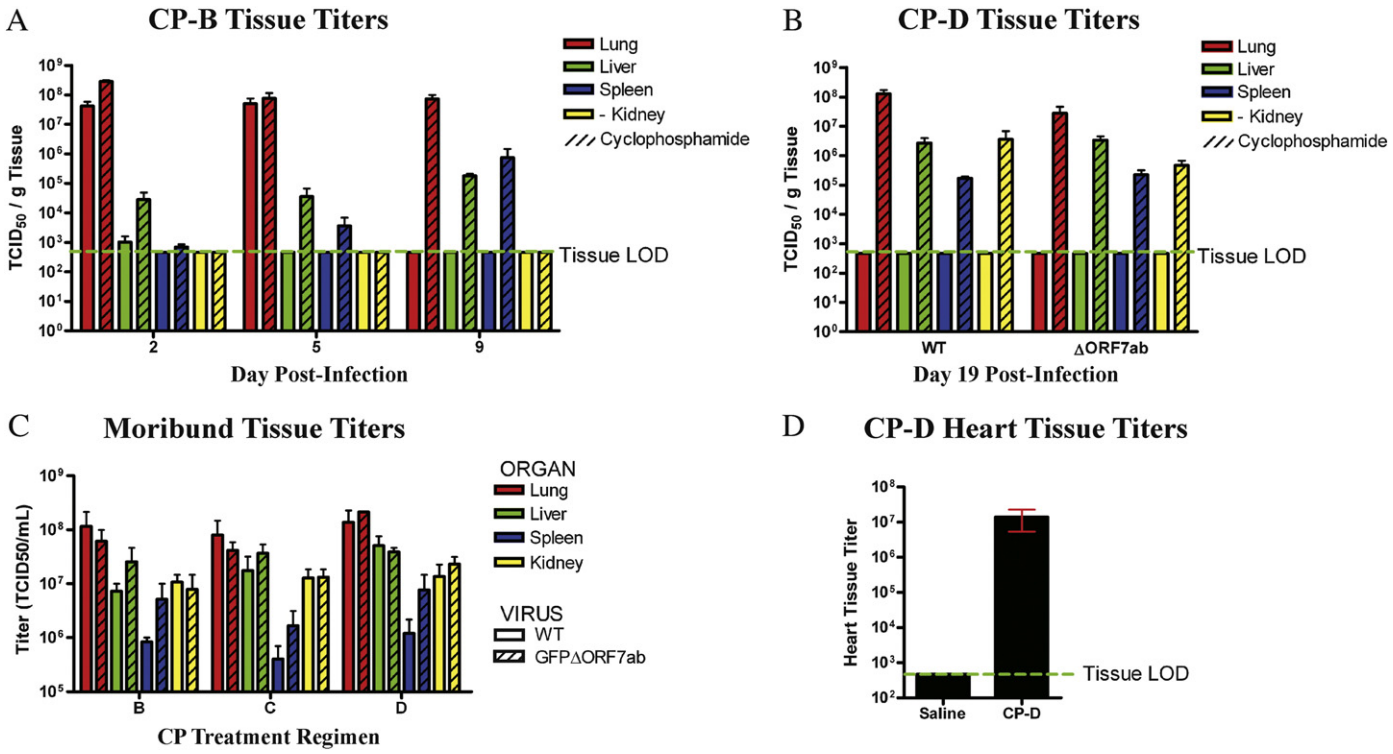

Fig. 3. SARS-CoV titers in tissues from immunosuppressed hamsters. (A) CP-B treated hamsters were infected intranasally with the indicated rSARS-CoV, sacrificed at the indicated times pi, and virus titers were measured in designated tissues. Open bars represent saline-treated animals; hashed bars represent CP-B treated hamsters. (B) CP-D treated hamsters were infected intranasally with either rSARS-CoV or rSARS-CoV ΔORF7ab virus. Animals were sacrificed at day 19 pi and virus titers were determined in the indicated tissues. Open bars represent saline-treated animals; hashed bars represent CP-D treated animals. (C) CP-B, CP-C, or CP-D treated hamsters were infected with rSARS-CoV or rSARS-CoV GFPΔORF7ab. Moribund animals were sacrificed and virus titers were measured in the indicated tissues. Mean days to moribundity for rSARS-CoV infected animals treated with CP-B, CP-C, and CP-D were 26.0 ($n=2$), 31.3 ($n=3$), and 25.3 ($n=3$), respectively. Mean days to death for rSARS-CoV GFPΔORF7ab infected animals treated with CP-B, CP-C, and CP-D were 26.5 ($n=2$), 31.0 ($n=3$), and 27.0 ($n=3$), respectively. $TCID_{50}$ limit of detection $=4.64\times10^2$ $TCID_{50}$/mL (D) CP-D treated hamsters were infected with rSARS-CoV or treated with saline. Moribund animals were sacrificed along with uninfected CP-D and age-matched saline-treated animals. Virus titer was determined in heart tissue. In all panels, virus titers from $n=3$ animals were determined by $TCID_{50}$.assay, and presented as means and standard error.

kidneys and urine of patients (Gu et al., 2005; Gu and Korteweg, 2007; Xu et al., 2005). No significant difference in virus titer was observed between wild-type and ORF7 deletion viruses in saline or CP-D treated animals.

Tissues harvested from moribund animals treated with CP-B, CP-C, and CP-D revealed high virus titers in the lungs, liver, spleen, and kidneys (Fig. 3C). All three treatments allowed for equivalent levels of virus replication. No significant difference was observed between rSARS-CoV and rSARS-CoV GFPΔORF7ab with respect to infectious virus titers in lung, liver, and kidney tissues ($P>0.05$). The rSARS-CoV GFPΔORF7ab virus-infected hamsters appeared to have higher virus titers in the spleen, but the difference was not statistically significant ($P=0.085$). Finally, heart tissues were analyzed for viral titers in saline-treated and moribund CP-D treated animals infected with rSARS-CoV (Fig. 3D). No virus was detected in hearts from saline-treated, infected animals; however, high viral titers were observed in the heart tissues from CP-D treated animals. Although the tissue specific expression of ACE2 (the cellular receptor for SARS-CoV) has not been determined in hamsters, ACE2 is expressed in heart, kidney, and testes in humans (Donoghue et al., 2000; Tipnis et al., 2000). The high viral titers in the hearts of these animals suggest that ACE2 is also present in heart tissues of hamsters. Of note, heart pathology has also been observed in human tissues from fatal SARS cases, including cardiac edema and atrophy of myocardial fibers (Chong et al., 2004; Ding et al., 2003; Gu et al., 2005; Lang et al., 2003).

Cyclophosphamide induced histopathology

A summary of histopathology due to CP treatment is shown in Table 2. At day 19 pi, administration of CP alone (CP-D) or in conjunction with virus challenge was associated with mild to marked hematopoietic atrophy in the bone marrow (femur and sternum), mild to moderate lymphoid depletion in the mandibular and/or mesenteric lymph nodes, moderate to marked lymphoid depletion in the spleen, and mild to moderate follicular atresia in the ovary, well-known consequences of CP administration in rodents (Jarrell et al., 1987). Atrophy of hematopoietic and lymphoid tissues is consistent with the chemotherapeutic and immunosuppressive pharmacology of CP. Hematopoietic atrophy was also evident in the bone marrow of CP-D treated and infected animals on day 5 pi, but was not evident on day 2 pi.

Two instances of necrotizing vaginitis were observed in hamsters treated with regimen CP-D; one of these was virus-infected and one was not. Since the incidence of this finding was low, a definitive relationship to CP administration was not certain; however, the finding is consistent with opportunistic bacterial infection following immunosuppression by CP.

Histopathological findings in cyclophosphamide treated, infected animals

Histopathological findings in saline-treated, rSARS-CoV infected animals were generally consistent with those previously described

Table 2
Histologic changes associated with cyclophosphamide

Tissue	Diagnosis	Group	1	2	3	4	5	6	Control	Control
		Sacrifice day	2	2	5	5	19	19	19	19
		Virus	+	+	+	+	+	+	−	−
		CP-D	−	+	−	+	−	+	−	+
		Severity								
Bone marrow, femur	Number examined		0	0	0	0	2	2	2	2
	No significant lesions						2	0	2	0
	Atrophy, hematopoietic	Minimal						1		
		Mild						1		1
		Moderate								
		Marked								1
Bone marrow, sternum	Number examined		2	2	2	2	2	2	2	2
	No significant lesions		2	2	2	0	2	0	2	0
	Atrophy, hematopoietic	Mild						2		1
		Moderate				2				1
	Hyperplasia, megakaryocytic	Mild								
Lymph node, mandibular	Number examined		0	0	0	0	2	2	2	2
	No significant lesions						2	0	2	0
	Depletion, lymphoid	Mild						1		2
		Moderate						1		
	Edema	Mild						2		2
		Moderate								
	Histiocytosis, sinus	Mild						2		1
	Hemorrhage, acute	Mild								1
Lymph node, mesenteric	Number examined		0	0	0	0	2	1	1	2
	No significant lesions						2	0	1	0
	Depletion, lymphoid	Mild								2
		Moderate						1		
	Hemorrhage, acute	Mild								
	Histiocytosis, sinus	Moderate								
	Edema	Mild								1
Ovary	Number examined		0	0	0	0	2	2	2	2
	No significant lesions						2	0	2	1
	Mineralization	Minimal						1		
	Delayed development	Mild								1
		Moderate						2		
Spleen	Number examined		0	0	0	0	1	2	2	1
	No significant lesions						1	0	1	0
	Depletion, lymphoid	Moderate						1		
		Marked						1		
Vagina	Number examined		0	0	0	0	2	2	2	2
	No significant lesions						2	1	2	1
	Vaginitis, necrotizing	Moderate								1
		Marked						1		

(Roberts et al., 2005b; 2006). rSARS-CoV infection of CP-D treated animals resulted in increased severity of histopathological findings in pulmonary and extrapulmonary tissues (summarized in Table 3).

Lung

At day 19 pi, chronic bronchointerstitial pneumonia of mild to moderate severity was observed in each of the hamsters infected with rSARS-CoV following immunosuppression with CP (Fig. 4A panel iii). Lesions were characterized by the presence of multifocal infiltrations of a mixed population of macrophages and neutrophils with lesser numbers of lymphocytes and plasma cells. Areas of fibrosis and hyperplasia of alveolar epithelial cells were frequently observed. Infiltration was centered at the junction between distal bronchioles and alveoli. At day 19 pi, this change was not present in the untreated, rSARS-CoV infected animals (Table 3).

Examination of lungs from animals given rSARS-CoV and CP at earlier times pi revealed the presence of moderate subacute bronchointerstitial pneumonia in one of two animals sacrificed at day 5 pi (Table 3; Fig. 4A panel ii); there were no meaningful changes present at day 2 pi. Histologically, the lesions were similar to the day 19 lesions in distribution, but lacked conspicuous fibrosis. Instead, hyperplasia of alveolar epithelial cells was a prominent feature at this earlier time point. Similar microscopic changes were also present in the lungs of both rSARS-CoV infected animals not treated with CP at day 5 (Table 3); no lesions were observed at day 2 pi.

Subacute inflammation of minimal severity was recorded for many animals in most treatment groups. Although this change was not observed in the small day 19 control groups, similar findings are extremely common in the lungs of hamsters of this age. Therefore, this change is not considered to represent a consequence of either rSARS-CoV or CP administration.

Heart

At day 19 pi, multifocal subacute myocardial inflammation of minimal severity was present in the hearts of two animals given rSARS-CoV and CP but not in saline-treated, infected animals (Fig. 4B; Table 3). This change consisted of infiltration by a mixed population of neutrophils, lymphocytes and macrophages occasionally surrounding degenerate or necrotic cardiac myocytes (Fig. 4B). Similar changes were not observed in the hearts of animals from earlier sacrifice intervals.

Nasal cavity

Fibrinopurulent exudate was visibly adherent to the mucosal surfaces at multiple levels of the nasal cavity in all animals inoculated with rSARS-CoV at days 2 and 5 pi (Table 3). There was no significant inflammatory cell infiltration within the submucosa of the nasal turbinates. Mild degeneration of olfactory epithelium was present in these regions. This change was present both in CP and saline-treated groups on days 2 and 5, but was observed only in CP-treated animals on day 19 pi (Fig. 4C).

Kidney

Dilation of renal cortical tubules or tubular degeneration and necrosis was present in the kidneys of infected, CP-D treated animals sacrificed on day 19 pi, but not in animals given only CP (Table 3). Each change was mild in severity and affected one of two animals.

No histological changes were noted in the gastrointestinal tract or the brain, therefore these tissues were not analyzed in subsequent experiments.

Histopathological findings in moribund animals

Based upon initial observations, target organs for virus-associated histopathology were considered to be the lung, heart, nasal turbinates, and the kidney. To determine the significance of these findings to morbidity and mortality of rSARS-CoV infected immunosuppressed hamsters, a follow-up study was conducted in which four animals were immunosuppressed using the CP-D regimen and inoculated with 10^3 $TCID_{50}$ of rSARS-CoV. Four animals given CP or saline only were used as controls. Animals were carefully monitored for evidence of moribundity or mortality; when observed, a matched number of control animals were sacrificed for comparison. From these animals, the following tissues were examined microscopically: heart, lung, spleen, kidney, bone marrow, and nasal turbinates (Table 4).

One rSARS-CoV infected, CP immunosuppressed animal was found dead on day 14 pi. Tissues from this animal exhibited changes comparable to those described above; however, this animal also had marked focal myocardial infarction with necrosis and bacteria, consistent with a septic myocardial infarct. Septicemic cardiac disease was interpreted as the cause death in this animal, and was likely secondary to immunosuppression by CP.

As with the initial study, CP treatment in the presence or absence of viral inoculation was associated with hematopoietic atrophy in the bone marrow and lymphoid depletion in the spleen.

In rSARS-CoV infected hamsters, inflammatory changes similar to those described above in the heart were present in all animals (Table 4). Histologically, inflammatory changes were more severe than those

Table 3
Histologic changes associated with SARS-CoV

Tissue	Diagnosis	Group	1	2	3	4	5	6	Control	Control
		Sacrifice day	2	2	5	5	19	19	19	19
		Virus	+	+	+	+	+	+	–	–
		CP-D	–	+	–	+	–	+	–	+
		Severity								
Heart	Number examined		2	2	2	2	2	2	2	2
	No significant lesions		2	2	2	2	2	0	2	2
	Inflammation, subacute	Minimal						2		
Kidney	Number examined		0	0	0	0	2	2	2	2
	No significant lesions						2	0	2	2
	Dilation, tubular	Mild						1		
	Degeneration/necrosis, tubular	Mild						1		
Lung	Number examined		2	2	2	2	2	2	2	2
	No significant lesions		0	1	0	0	0	0	2	2
	Inflammation, subacute	Minimal	2	1		1	2			
	Pneumonia, bronchointerstitial	Mild						1		
		Moderate			2	1		1		
Nasal turbinate	Number examined		2	2	2	2	2	2	2	2
	No significant lesions		0	0	0	0	2	0	2	2
	Exudate, fibrinopurulent	Minimal						1		
		Mild		1	1	1		1		
		Moderate	2	1	1	1				

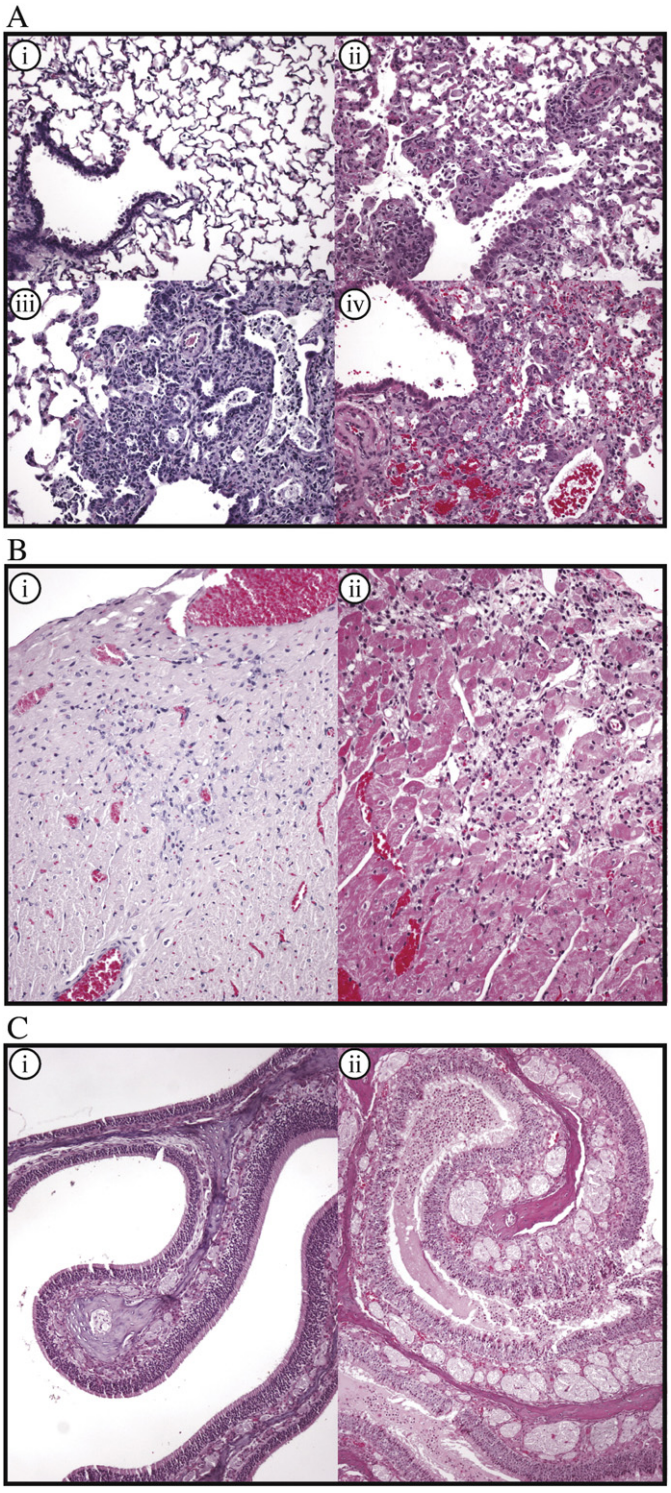

Fig. 4. Histopathology of SARS-CoV infected hamsters. Hematoxylin and eosin (H and E) stain of pulmonary and extrapulmonary tissues. (A) Histopathologic lesions in the lungs of rSARS-CoV infected hamsters treated with CP-D. (i) Bronchoalveolar junction of control animal lung. (ii, iii, iv) Temporal changes in the lung of hamsters at 5, 19, and 23 days pi, respectively. In animals sacrificed moribund (n=1 at day 23 pi and n=2 at day 24 pi) (iv), changes were severe, widespread and frequently associated with hemorrhage. (B) Myocardium sections of (i) uninfected and (ii) rSARS-CoV infected, CP-D treated hamsters at 19 days pi. Subacute inflammation in the myocardium was present in rSARS-CoV infected animals, as well as in those animals sacrificed moribund. (C) Nasal turbinates of (i) uninfected and (ii) rSARS-CoV infected, CP-D treated hamsters 19 days pi.

Table 4
Histologic findings in moribund animals

Tissue	Diagnosis	Group	1	2	Control
		Virus	+	−	−
		CP-D	+	+	−
		Severity			
Bone marrow	Number examined		4	4	4
	No significant lesions		0	0	4
	Atrophy, hematopoietic	Mild	4	3	
		Moderate		1	
Heart	Number examined		4	4	4
	No significant lesions		0	4	4
	Epicarditis, subacute	Marked	4	3	
	Inflammation, subacute	Mild	1		
		Moderate	3		
	Infarction, myocardial	Moderate	1		
Kidney	Number examined		4	4	4
	No significant lesions		0	4	3
	Degeneration/necrosis, tubular	Minimal	1		
		Mild	2		
		Moderate	1		
	Dilation, tubular	Mild			1
Lung	Number examined		4	4	4
	No significant lesions		0	2	4
	Pneumonia, bronchointerstitial	Moderate	1		
		Marked	3		
	Pleuritis, subacute	Marked	1		
	Histiocytosis, alveolar	Minimal		2	
Nasal turbinates	Number examined		4	4	4
	No significant lesions		0	4	4
	Exudate, fibrinopurulent	Mild	2		
		Moderate	2		
Spleen	Number examined		4	4	4
	No significant lesions		0	0	4
	Depletion, lymphoid	Marked	4	4	

observed on day 19 pi. In the three animals surviving to days 23 and 24 pi, severe pulmonary lesions were observed, representing an increasing consolidation and histologic severity from lesions observed on day 19 pi. There was extensive pulmonary hemorrhage and edema in the lungs of these animals (Table 4). All rSARS-CoV infected animals exhibited minimal to moderate renal tubular degeneration and necrosis and fibrinopurulent exudation within nasal turbinates similar to that described above (Table 4).

Discussion

The lack of a small animal model that more closely resembles human SARS-CoV infection has restricted the study of SARS-CoV pathogenesis, vaccine design, and analysis of antiviral therapies in vivo. Pathological analysis of the respiratory tracts of SARS patients revealed diffuse alveolar damage, hyaline membrane formation and interstitial edema. Extrapulmonary pathology included splenic lymphocyte depletion and atrophy, acute tubular necrosis in kidneys, neuronal edema and degeneration, heart edema and myocardial fiber atrophy, and minor pathological changes in bone marrow, skeletal muscle, adrenal and thyroid glands, and testes (reviewed in Gu and Korteweg, 2007). Viral particles and viral genomes were detected in numerous tissues and cell types including the respiratory epithelium, circulating lymphocytes, monocytes, lymphoid tissues, intestinal mucosal epithelium, renal distal tubule epithelial cells, neurons of the brain, and macrophages in multiple organs (Gu et al., 2005). An ideal small animal model would encompass many of the characteristics of human infection, including severe pulmonary disease, spread of virus to extrapulmonary organs and tissues, histopathology reminiscent of human infection, overt clinical symptoms, a longer time period of infection and mortality.

BALB/c and C57BL/6 mice have been predominantly utilized for small animal infection studies. SARS-CoV inoculation in these mouse strains demonstrates moderate replication in nasal turbinates and

lungs; however, peak titers occur at days 2–3 pi and virus is cleared by days 5–7 pi (Glass et al., 2004; Hogan et al., 2004; Roberts et al., 2005a; Subbarao et al., 2004). Infected mice do not display overt clinical disease and demonstrate no morbidity or mortality. An aged BALB/c mouse model has been described that demonstrates some observable morbidity including weight loss, ruffled fur, and increased histopathological findings (Roberts et al., 2005a). No mortality was observed. STAT1$^{-/-}$ 129SvEv mice were analyzed as a potential animal model and displayed a prolonged infection period with extrapulmonary spread to the liver and spleen, and histopathological findings of acute interstitial pneumonia (Hogan et al., 2004), although no mortality was reported. The first murine models that demonstrated severe disease and mortality utilized C57BL/6 and C57BL/6×C3H/HeJ mice transgenic for human ACE2, the SARS-CoV cellular receptor (McCray et al., 2007; Tseng et al., 2007). Infection of the transgenic mice resulted in a severe and rapid progression of disease with 100% mortality by day 7–8 pi. Virus replication was detected in several organs with high virus titers in the brain by day 3. Although potentially useful for pathogenesis studies, the severe and rapid nature of disease coupled with the prominent, neurologic involvement may constrain their usefulness as a small animal model for SARS-CoV. Additionally, a mouse-adapted strain of SARS-CoV has been generated via 15 serial passages through BALB/c mice (Roberts et al., 2007). This virus is capable of causing severe disease in mice with extrapulmonary spread; however, as with the transgenic ACE2 mice, the disease is rapid causing death within 5 days of inoculation.

The results of this study demonstrate that CP-induced immunosuppression of Syrian golden hamsters significantly increases the severity of SARS-CoV disease. Although hamsters are permissive to SARS-CoV infection, animals demonstrate minimal clinical illness and weight loss, and no mortality is observed (Roberts et al., 2005b). The use of CP to induce an immunosuppressed state results in a significant increase in viral pathology, increased weight loss, expanded tissue tropism and a prolonged time frame for disease.

A low dose CP regimen (CP-A) led to prolonged virus replication in the lungs, and other organs, but only moderate weight loss and no mortality. Since the effects of CP are primarily on lymphoid cell populations, this data suggests the involvement of this cell type in the control and clearance of SARS-CoV in the lung. Increasing the CP dose and frequency resulted in a significant increase in pathology and mortality. CP-B treatment resulted in an 83% mortality rate, whereas 100% of CP-C and CP-D infected animals died within approximately 30 days of rSARS-CoV infection. High virus titers were observed in numerous tissues from the CP-B, CP-C, and CP-D treated animals, including lung, liver, spleen, kidney, and heart.

Infection with rSARS-CoV was associated with acute fibrinopurulent exudation in the nasal cavity and renal tubular degeneration/necrosis regardless of the presence or absence of CP immunosuppression. Additionally, rSARS-CoV infection following CP-D immunosuppression produced bronchointerstitial pneumonia which progressed in severity over the duration of the experiment. Subacute inflammation of the ventricular myocardium was observed in immunosuppressed, rSARS-CoV infected animals, with increasing severity being observed between days 19 and 23/24 pi. The latter changes (chronic bronchointerstitial pneumonia and myocardial inflammation) likely contributed to the severity of clinical disease necessitating sacrifice of moribund animals 23–24 days pi. It is important to note that we did not see pathology in the gastrointestinal tract or in the brain of any SARS-CoV infected hamsters. SARS-CoV has been associated with gastrointestinal tissue in human autopsies and mice expressing the human ACE2 receptor show symptoms of encephalitis after SARS-CoV infection. The significance of SARS-CoV infectin of the brain and gastrointestinal tract is not clear and remains an open area of investigation.

Although this immunosuppressed model will not likely be useful for vaccine studies, it may be of significant utility in analysis of the virulence of recombinant viruses and in assessing the efficacy of antiviral compounds or treatments. In this study, we have analyzed the in vivo replication and pathogenesis of two recombinant SARS-CoV strains with deletions of the ORF7ab region. rSARS-CoV ΔORF7ab viruses can replicate with wild-type efficiency in vitro and in mouse models of SARS-CoV infection (Dediego et al., 2008; Schaecher et al., 2007b; Sims et al., 2005; Yount et al., 2005). Together these data suggest that the SARS-CoV ORF7a and ORF7b proteins are not required for viral replication in the small animal models described to date, but may provide luxury functions in other host species. It will be important to test a number of other recombinant viruses bearing disruption of other accessory genes in the immunosuppressed hamster model.

It is not clear if the increased pathology observed in CP-treated, infected animals is due to increased virus replication, prolonged virus replication or to increased damage from cytokines induced by the infection. Reagents for cytokine analysis in hamsters are lacking but this is clearly an important area of future research. The efficacy of antiviral or immunotherapies in protecting CP-treated hamsters from SARS-CoV disease will be important to assess, as the increased virus replication and spread of virus to extrapulmonary sites provides a more rigorous test of treatment efficacy.

Materials and methods

Cells

Vero (ATCC CRL-1586) cells were cultured in complete medium (Dulbecco's modified Eagle medium containing 10% fetal bovine serum [Atlanta Biologicals], 1 mM glutamine [Gibco], 1 mM sodium pyruvate [Cellgro], 100 U/mL penicillin [Gibco], and 100 μg/mL streptomycin [Gibco]). Cells were incubated in a 5% CO2 humidified incubator at 37 °C.

Viruses

Recombinant SARS-CoVs were kindly provided by Ralph Baric, University of North Carolina. Either recombinant, wild-type SARS-CoV (rSARS-CoV), virus with GFP in place of the gene 7 coding region (rSARS-CoV GFPΔORF7ab), or virus with the gene 7 region fully deleted (rSARS-CoV ΔORF7ab) was used. Briefly, nucleotides 27276 to 27643 (accession number A278741) were either deleted or replaced with the ORF for GFP, and recombinant viruses generated as previously described (Sims et al., 2005; Yount et al., 2003; 2005). The viruses were propagated and virus titers determined as previously described (Nelson et al., 2005; Schaecher et al., 2007a). All infections were performed in a biosafety level 3 laboratory using Institutional Biosafety Committee approved procedures.

Cyclophosphamide treatment and infection of Syrian golden hamsters

Six to seven week-old Syrian golden hamsters (Charles River Laboratories) were housed three per cage in a biosafety level 3 animal facility. CP (Sigma) was dissolved in 0.9% saline with vigorous shaking to make a stock solution of 21 mg/mL. Animals were injected IP with 0.8 mL of saline or 0.2–0.8 mL of CP to the desired concentration and per the dosing schedule detailed in Table 1 to maintain immunosuppression.

Animals were acclimatized in the ABSL-3 biosafety containment rack for at least 7 days, and then inoculated with PBS or 10^3 $TCID_{50}$ of virus in a total volume of 100 μL (50 μL into each naris). Hamsters were weighed at the indicated times pi.

CP-induced immunosuppression was monitored by total white blood cell (WBC) counts utilizing using a Pentra 60 Hematology Analyzer (ABX Diagnostics, Montpellier, France) per the manufacturer's protocol for samples collected before virus infection. A

manual differential cell count was also performed on samples collected after virus infection using a blood smear and modified Wright's stain. Ten fields of cells were counted at a 10× magnification per sample.

Hamsters were sacrificed on the indicated days pi, and virus titers in homogenates of lung, kidney, liver, spleen, and heart tissues were determined (Rowe et al., 2004b). Tissues were weighed, complete medium was added to achieve a 10% weight to volume (wt/vol) suspension, and homogenized using tissue grinders (Fisher). After centrifugation at 3400 rpm for 10 min, the supernatants were removed and analyzed by $TCID_{50}$ assay. All procedures were performed under protocols approved by the Institutional Biosafety and the Institutional Animal Care and Use Committees.

Neutralizing antibody analysis

Animal sera was collected from infected animals at days 19 and 42 pi and assayed for the presence of anti-SARS-CoV neutralizing antibodies essentially as described by others (Subbarao et al., 2004). Briefly, serum was heat inactivated at 55 °C for 30 min. Two-fold dilutions of inactivated sera were mixed in complete media to a final volume of 100 μL per well and 100 $TCID_{50}$ of SARS-CoV per 100 μL sera-containing media was added. The antisera-virus suspension was pre-incubated at 25 °C for 30 min. 100 μL was added to each of 6 wells of Vero cell monolayers in a 96 well plate per serum dilution. Cells were fixed with 1% formaldehyde 4 days pi, stained with Napthol Blue-Black (Sigma), and analyzed for cytopathic effect. The dilution of serum that prevented cytopathic effect in 50% of wells was calculated using the Reed-Muench formula (Reed and Muench, 1938).

Histopathology

Formalin-fixed tissues were embedded in paraffin and 4–5 μm thick sections were generated with a microtome and stained with hematoxylin and eosin. The CP-D treatment regimen was used for all histopathological studies. The following tissues were harvested at day 19 pi: adrenal gland, aorta, bone (femur), bone (sternum), bone marrow (femur), bone marrow (sternum), brain, cecum, cervix, colon, duodenum, esophagus, eye, gall bladder, Harderian gland, heart, ileum, jejunum, kidney, larynx, liver, lung, mammary gland, mandibular lymph node, mesenteric lymph node, nasal cavity (3 levels), optic nerve, ovary, pancreas, parathyroid, pituitary gland, rectum, salivary gland, skeletal muscle, skin, spinal cord, spleen, stomach, thymus, thyroid, tongue, trachea, urinary bladder, uterus, and vagina. Tissues from two animals per condition were assessed. Based on findings from this full survey of tissues, tissues including bone marrow (sternum or tibia), heart, lung, kidney, spleen and nasal cavity (2 animals per group) were examined at the indicated days postinfection in subsequent experiments.

Acknowledgments

We thank all the members of the Pekosz and Buller laboratories for their insightful discussions and comments. We also thank Michael Diamond and the Diamond laboratory for support and helpful discussions. We acknowledge and thank Ralph Baric, University of North Carolina, for generously providing the recombinant SARS-CoV strains used in this study.

This study was supported by the Markey Pathway (S.R.S.), T32 HL07317 (S.R.S.), AI059328 (A.P.), the Eliasberg Foundation (A.P.), the Marjorie Gilbert Foundation (A.P.), NOI-AI-15436 (R.M.B.), and U54-AI-057160 (R.M.B.+A.P.) from the NIAID to the Midwestern Regional Center of Excellence for Biodefense and Emerging Infectious Diseases (MRCE).

References

Blandford, G., Charlton, D., 1977. Studies of pulmonary and renal immunopathology after nonlethal primary sendai viral infection in normal and cyclophosphamide-treated hamsters. Am. Rev. Respir. Dis. 115 (2), 305–314.

CDC, 2003. Revised U.S. surveillance case definition for severe acute respiratory syndrome (SARS) and update on SARS cases—United States and worldwide, December 2003. MMWR. Morb. Mortal. Wkly. Rep. 52 (49), 1202–1206.

Chan, K.H., Poon, L.L., Cheng, V.C., Guan, Y., Hung, I.F., Kong, J., Yam, L.Y., Seto, W.H., Yuen, K.Y., Peiris, J.S., 2004a. Detection of SARS coronavirus in patients with suspected SARS. Emerg. Infect. Dis. 10 (2), 294–299.

Chan, W.M., Kwan, Y.W., Wan, H.S., Leung, C.W., Chiu, M.C., 2004b. Epidemiologic linkage and public health implication of a cluster of severe acute respiratory syndrome in an extended family. Pediatr. Infect. Dis. J. 23 (12), 1156–1159.

Cheng, V.C., Lau, S.K., Woo, P.C., Yuen, K.Y., 2007. Severe acute respiratory syndrome coronavirus as an agent of emerging and reemerging infection. Clin. Microbiol. Rev. 20 (4), 660–694.

Chong, P.Y., Chui, P., Ling, A.E., Franks, T.J., Tai, D.Y., Leo, Y.S., Kaw, G.J., Wansaicheong, G., Chan, K.P., Ean Oon, L.L., Teo, E.S., Tan, K.B., Nakajima, N., Sata, T., Travis, W.D., 2004. Analysis of deaths during the severe acute respiratory syndrome (SARS) epidemic in Singapore: challenges in determining a SARS diagnosis. Arch. Pathol. Lab. Med. 128 (2), 195–204.

Cupps, T.R., Edgar, L.C., Fauci, A.S., 1982. Suppression of human B lymphocyte function by cyclophosphamide. J. Immunol. 128 (6), 2453–2457.

Dediego, M.L., Pewe, L., Alvarez, E., Rejas, M.T., Perlman, S., Enjuanes, L., 2008. Pathogenicity of severe acute respiratory coronavirus deletion mutants in hACE-2 transgenic mice. Virology.

Ding, Y., Wang, H., Shen, H., Li, Z., Geng, J., Han, H., Cai, J., Li, X., Kang, W., Weng, D., Lu, Y., Wu, D., He, L., Yao, K., 2003. The clinical pathology of severe acute respiratory syndrome (SARS): a report from China. J. Pathol. 200 (3), 282–289.

Donoghue, M., Hsieh, F., Baronas, E., Godbout, K., Gosselin, M., Stagliano, N., Donovan, M., Woolf, B., Robison, K., Jeyaseelan, R., Breitbart, R.E., Acton, S., 2000. A novel angiotensin-converting enzyme-related carboxypeptidase (ACE2) converts angiotensin I to angiotensin 1–9. Circ. Res. 87 (5), E1–E9.

Fouchier, R.A., Kuiken, T., Schutten, M., Van Amerongen, G., Van Doornum, G.J., Van Den Hoogen, B.G., Peiris, M., Lim, W., Stohr, K., Osterhaus, A.D., 2003. Aetiology: Koch's postulates fulfilled for SARS virus. Nature 423 (6937), 240.

Genovesi, E.V., Peters, C.J., 1987. Immunosuppression-induced susceptibility of inbred hamsters (*Mesocricetus auratus*) to lethal-disease by lymphocytic choriomeningitis virus infection. Arch. Virol. 97 (1–2), 61–76.

Glass, W.G., Subbarao, K., Murphy, B., Murphy, P.M., 2004. Mechanisms of host defense following severe acute respiratory syndrome-coronavirus (SARS-CoV) pulmonary infection of mice. J. Immunol. 173 (6), 4030–4039.

Greenough, T.C., Carville, A., Coderre, J., Somasundaran, M., Sullivan, J.L., Luzuriaga, K., Mansfield, K., 2005. Pneumonitis and multi-organ system disease in common marmosets (*Callithrix jacchus*) infected with the severe acute respiratory syndrome-associated coronavirus. Am. J. Pathol. 167 (2), 455–463.

Gu, J., Korteweg, C., 2007. Pathology and pathogenesis of severe acute respiratory syndrome. Am. J. Pathol. 170 (4), 1136–1147.

Gu, J., Gong, E., Zhang, B., Zheng, J., Gao, Z., Zhong, Y., Zou, W., Zhan, J., Wang, S., Xie, Z., Zhuang, H., Wu, B., Zhong, H., Shao, H., Fang, W., Gao, D., Pei, F., Li, X., He, Z., Xu, D., Shi, X., Anderson, V.M., Leong, A.S.Y., 2005. Multiple organ infection and the pathogenesis of SARS. J. Exp. Med. 202 (3), 415–424.

Ho, M.S., Chen, W.J., Chen, H.Y., Lin, S.F., Wang, M.C., Di, J., Lu, Y.T., Liu, C.L., Chang, S.C., Chao, C.L., King, C.C., Chiou, J.M., Su, I.J., Yang, J.Y., 2005. Neutralizing antibody response and SARS severity. Emerg. Infect. Dis. 11 (11), 1730–1737.

Hogan, R.J., Gao, G., Rowe, T., Bell, P., Flieder, D., Paragas, J., Kobinger, G.P., Wivel, N.A., Crystal, R.G., Boyer, J., Feldmann, H., Voss, T.G., Wilson, J.M., 2004. Resolution of primary severe acute respiratory syndrome-associated coronavirus infection requires Stat1. J. Virol. 78 (20), 11416–11421.

Ikezawa, Y., Nakazawa, M., Tamura, C., Takahashi, K., Minami, M., Ikezawa, Z., 2005. Cyclophosphamide decreases the number, percentage and the function of CD25+ CD4+ regulatory T cells, which suppress induction of contact hypersensitivity. J. Dermatol. Sci. 39 (2), 105–112.

Jarrell, J., Lai, E.V., Barr, R., McMahon, A., Belbeck, L., O'Connell, G., 1987. Ovarian toxicity of cyclophosphamide alone and in combination with ovarian irradiation in the rat. Cancer. Res. 47 (9), 2340–2343.

Kercher, L., Mitchell, B.M., 2000. Immune transfer protects severely immunosuppressed mice from murine cytomegalovirus retinitis and reduces the viral load in ocular tissue. J. Infect. Dis. 182 (3), 652–661.

Kong, X., Hellermann, G.R., Patton, G., Kumar, M., Behera, A., Randall, T.S., Zhang, J., Lockey, R.F., Mohapatra, S.S., 2005. An immunocompromised BALB/c mouse model for respiratory syncytial virus infection. Virol. J. 2, 3.

Lang, Z.W., Zhang, L.J., Zhang, S.J., Meng, X., Li, J.Q., Song, C.Z., Sun, L., Zhou, Y.S., Dwyer, D.E., 2003. A clinicopathological study of three cases of severe acute respiratory syndrome (SARS). Pathology 35 (6), 526–531.

Lau, S.K.P., Woo, P.C.Y., Li, K.S.M., Huang, Y., Tsoi, H.-W., Wong, B.H.L., Wong, S.S.Y., Leung, S.Y., Chan, K.H., Yuen, K.Y., 2005. Severe acute respiratory syndrome coronavirus-like virus in Chinese horseshoe bats. PNAS 102 (39), 14040–14045.

Lawler, J.V., Endy, T.P., Hensley, L.E., Garrison, A., Fritz, E.A., Lesar, M., Baric, R.S., Kulesh, D.A., Norwood, D.A., Wasieloski, L.P., Ulrich, M.P., Slezak, T.R., Vitalis, E., Huggins, J.W., Jahrling, P.B., and Paragas, J., (2006). Cynomolgus macaque as an animal model for severe acute respiratory syndrome. *PLoS Medicine* 3(5), doi:10.1371/journal.pmed.0030149.

Li, W., Shi, Z., Yu, M., Ren, W., Smith, C., Epstein, J.H., Wang, H., Crameri, G., Hu, Z., Zhang, H., Zhang, J., McEachern, J., Field, H., Daszak, P., Eaton, B.T., Zhang, S., Wang, L.F.,

2005. Bats are natural reservoirs of SARS-like coronaviruses. Science 310 (5748), 676–679.
Martina, B.E., Haagmans, B.L., Kuiken, T., Fouchier, R.A., Rimmelzwaan, G.F., Van Amerongen, G., Peiris, J.S., Lim, W., Osterhaus, A.D., 2003. Virology: SARS virus infection of cats and ferrets. Nature 425 (6961), 915.
Mateo, R., Xiao, S.Y., Guzman, H., Lei, H.A.O., Da Rosa, A.P.A.T., Tesh, R.B., 2006. Effects of immunosuppression on West Nile virus infection in hamsters. Am. J. Trop. Med. Hyg. 75 (2), 356–362.
McAuliffe, J., Vogel, L., Roberts, A., Fahle, G., Fischer, S., Shieh, W.J., Butler, E., Zaki, S., St Claire, M., Murphy, B., Subbarao, K., 2004. Replication of SARS coronavirus administered into the respiratory tract of African Green, rhesus and cynomolgus monkeys. Virology 330 (1), 8–15.
McCray Jr., P.B., Pewe, L., Wohlford-Lenane, C., Hickey, M., Manzel, L., Shi, L., Netland, J., Jia, H.P., Halabi, C., Sigmund, C.D., Meyerholz, D.K., Kirby, P., Look, D.C., Perlman, S., 2007. Lethal infection of K18-hACE2 mice infected with severe acute respiratory syndrome coronavirus. J. Virol. 81 (2), 813–821.
Nelson, C.A., Pekosz, A., Lee, C.A., Diamond, M.S., Fremont, D.H., 2005. Structure and intracellular targeting of the SARS-coronavirus Orf7a accessory protein. Structure (Camb) 13 (1), 75–85.
Polak, L., Turk, J.L., 1974. Reversal of immunological tolerance by cyclophosphamide through inhibition of suppressor cell activity. Nature 249 (458), 654–656.
Poon, L.L., Chan, K.H., Wong, O.K., Cheung, T.K., Ng, I., Zheng, B., Seto, W.H., Yuen, K.Y., Guan, Y., Peiris, J.S., 2004. Detection of SARS coronavirus in patients with severe acute respiratory syndrome by conventional and real-time quantitative reverse transcription-PCR assays. Clin. Chem. 50 (1), 67–72.
Qin, C., Wang, J., Wei, Q., She, M., Marasco, W.A., Jiang, H., Tu, X., Zhu, H., Ren, L., Gao, H., Guo, L., Huang, L., Yang, R., Cong, Z., Guo, L., Wang, Y., Liu, Y., Sun, Y., Duan, S., Qu, J., Chen, L., Tong, W., Ruan, L., Liu, P., Zhang, H., Zhang, J., Zhang, H., Liu, D., Liu, Q., Hong, T., He, W., 2005. An animal model of SARS produced by infection of *Macaca mulatta* with SARS coronavirus. J. Pathol. 206 (3), 251–259.
Reed, L.J., Muench, H., 1938. A simple method of estimating 50 percent endpoints. Am. J. Hyg. 27, 493–499.
Ren, W., Li, W., Yu, M., Hao, P., Zhang, Y., Zhou, P., Zhang, S., Zhao, G., Zhong, Y., Wang, S., Wang, L.-F., Shi, Z., 2006. Full-length genome sequences of two SARS-like coronaviruses in horseshoe bats and genetic variation analysis. J. Gen. Virol. 87 (11), 3355–3359.
Roberts, A., Paddock, C., Vogel, L., Butler, E., Zaki, S., Subbarao, K., 2005a. Aged BALB/c mice as a model for increased severity of severe acute respiratory syndrome in elderly humans. J. Virol. 79 (9), 5833–5838.
Roberts, A., Vogel, L., Guarner, J., Hayes, N., Murphy, B., Zaki, S., Subbarao, K., 2005b. Severe acute respiratory syndrome coronavirus infection of golden Syrian hamsters. J. Virol. 79 (1), 503–511.
Roberts, A., Thomas, W.D., Guarner, J., Lamirande, E.W., Babcock, G.J., Greenough, T.C., Vogel, L., Hayes, N., Sullivan, J.L., Zaki, S., Subbarao, K., Ambrosino, D.M., 2006. Therapy with a severe acute respiratory syndrome-associated coronavirus-neutralizing human monoclonal antibody reduces disease severity and viral burden in golden Syrian hamsters. J. Infect. Dis. 193 (5), 685–692.
Roberts, A., Deming, D., Paddock, C.D., Cheng, A., Yount, B., Vogel, L., Herman, B.D., Sheahan, T., Heise, M., Genrich, G.L., Zaki, S.R., Baric, R., Subbarao, K., 2007. A Mouse-Adapted SARS-coronavirus causes disease and mortality in BALB/c mice. PLoS. Pathogens. 3 (1), e5.
Roberts, A., Lamirande, E.W., Vogel, L., Jackson, J.P., Paddock, C.D., Guarner, J., Zaki, S.R., Sheahan, T., Baric, R., Subbarao, K., 2008. Animal models and vaccines for SARS-CoV infection. Virus. Res. 133 (1), 20–32.
Rowe, R.K., Brody, S.L., Pekosz, A., 2004a. Differentiated cultures of primary hamster tracheal airway epithelial cells. In Vitro Cell. Dev. Biol. Anim. 40 (10), 303–311.
Rowe, T., Gao, G., Hogan, R.J., Crystal, R.G., Voss, T.G., Grant, R.L., Bell, P., Kobinger, G.P., Wivel, N.A., Wilson, J.M., 2004b. Macaque model for severe acute respiratory syndrome. J. Virol. 78 (20), 11401–11404.
Schaecher, S.R., Mackenzie, J.M., Pekosz, A., 2007a. The ORF7b protein of severe acute respiratory syndrome coronavirus (SARS-CoV) is expressed in virus-infected cells and incorporated into SARS-CoV particles. J. Virol. 81 (2), 718–731.
Schaecher, S.R., Touchette, E., Schriewer, J., Buller, R.M., Pekosz, A., 2007b. Severe acute respiratory syndrome coronavirus gene 7 products contribute to virus-induced apoptosis. J. Virol. 81 (20), 11054–11068.
Sidwell, R.W., Bailey, K.W., Morrey, J.D., Wong, M.H., Baldwin, T.J., Smee, D.F., 2003. Inhibition of influenza virus infections in immunosuppressed mice with orally administered peramivir (BCX-1812). Antiviral Res. 60 (1), 17–25.
Sims, A.C., Baric, R.S., Yount, B., Burkett, S.E., Collins, P.L., Pickles, R.J., 2005. Severe acute respiratory syndrome coronavirus infection of human ciliated airway epithelia: role of ciliated cells in viral spread in the conducting airways of the lungs. J. Virol. 79 (24), 15511–15524.
Smee, D.F., Burger, R.A., Coombs, J., Huffman, J.H., Sidwell, R.W., 1991. Progressive murine cytomegalovirus disease after termination of ganciclovir therapy in mice immunosuppressed by cyclophosphamide treatment. J. Infect. Dis. 164 (5), 958–961.
Subbarao, K., McAuliffe, J., Vogel, L., Fahle, G., Fischer, S., Tatti, K., Packard, M., Shieh, W.J., Zaki, S., Murphy, B., 2004. Prior infection and passive transfer of neutralizing antibody prevent replication of severe acute respiratory syndrome coronavirus in the respiratory tract of mice. J. Virol. 78 (7), 3572–3577.
ter Meulen, J., Bakker, A.B.H., van den Brink, E.N., Weverling, G.J., Martina, B.E.E., Haagmans, B.L., Kuiken, T., de Kruif, J., Preiser, W., Spaan, W., 2004. Human monoclonal antibody as prophylaxis for SARS coronavirus infection in ferrets. The Lancet 363 (9427), 2139–2141.
Tipnis, S.R., Hooper, N.M., Hyde, R., Karran, E., Christie, G., Turner, A.J., 2000. A human homolog of angiotensin-converting enzyme. Cloning and functional expression as a captopril-insensitive carboxypeptidase. J. Biol. Chem. 275 (43), 33238–33243.
Toth, K., Spencer, J.F., Dhar, D., Sagartz, J.E., Buller, R.M., Painter, G.R., Wold, W.S., 2008. Hexadecyloxypropyl-cidofovir, CMX001, prevents adenovirus-induced mortality in a permissive, immunosuppressed animal model. Proc. Natl. Acad. Sci. U. S. A. 105 (20), 7293–7297.
Tseng, C.-T.K., Huang, C., Newman, P., Wang, N., Narayanan, K., Watts, D.M., Makino, S., Packard, M.M., Zaki, S.R., Chan, T.-S., Peters, C.J., 2007. Severe acute respiratory syndrome coronavirus infection of mice transgenic for the human angiotensin-converting enzyme 2 virus receptor. J. Virol 81 (3), 1162–1173.
Wu, D., Tu, C., Xin, C., Xuan, H., Meng, Q., Liu, Y., Yu, Y., Guan, Y., Jiang, Y., Yin, X., Crameri, G., Wang, M., Li, C., Liu, S., Liao, M., Feng, L., Xiang, H., Sun, J., Chen, J., Sun, Y., Gu, S., Liu, N., Fu, D., Eaton, B.T., Wang, L.-F., Kong, X., 2005. Civets are equally susceptible to experimental infection by two different severe acute respiratory syndrome coronavirus isolates. J. Virol. 79 (4), 2620–2625.
Xu, D., Zhang, Z., Jin, L., Chu, F., Mao, Y., Wang, H., Liu, M., Wang, M., Zhang, L., Gao, G.F., Wang, F.S., 2005. Persistent shedding of viable SARS-CoV in urine and stool of SARS patients during the convalescent phase. Eur. J. Clin. Microbiol. Infect. Dis. 24 (3), 165–171.
Yount, B., Curtis, K.M., Fritz, E.A., Hensley, L.E., Jahrling, P.B., Prentice, E., Denison, M.R., Geisbert, T.W., Baric, R.S., 2003. Reverse genetics with a full-length infectious cDNA of severe acute respiratory syndrome coronavirus. PNAS 100 (22), 12995–13000.
Yount, B., Roberts, R.S., Sims, A.C., Deming, D., Frieman, M.B., Sparks, J., Denison, M.R., Davis, N., Baric, R.S., 2005. Severe acute respiratory syndrome coronavirus group-specific open reading frames encode nonessential functions for replication in cell cultures and mice. J. Virol. 79 (23), 14909–14922.
Zhang, L., Zhang, F., Yu, W., He, T., Yu, J., Yi, C.E., Ba, L., Li, W., Farzan, M., Chen, Z., Yuen, K. Y., Ho, D., 2006. Antibody responses against SARS coronavirus are correlated with disease outcome of infected individuals. J. Med. Virol. 78 (1), 1–8.
Zhu, L.P., Cupps, T.R., Whalen, G., Fauci, A.S., 1987. Selective effects of cyclophosphamide therapy on activation, proliferation, and differentiation of human B cells. J. Clin. Invest. 79 (4), 1082–1090.